J Appl Electrochem (2009) 39:617–625
DOI 10.1007/s10800-008-9699-8

ORIGINAL PAPER

Electrochemical properties of $Li_{1-z}(Ni_{1-y}Fe_y)_{1+z}O_2$ synthesized by the combustion method in an air atmosphere

Myoung Youp Song · Ik Hyun Kwon · Jiunn Song · Sungbo Shim

Received: 16 February 2008 / Accepted: 20 October 2008 / Published online: 5 November 2008

Abstract For the syntheses of $LiNi_{1-y}Fe_yO_2$ ($0.000 \leq y \leq 0.300$), mixtures of the starting materials with the desired compositions were preheated in an air atmosphere at 400 °C for 30 min and calcined in air at 700 °C for 48 h. The phases appearing in the intermediate reaction steps for the formation of lithium nickel oxide are deduced from the DTA analysis. XRD analysis, FE-SEM observation, FTIR analysis and electrochemical measurement were performed for the synthesized $Li_{1-z}(Ni_{1-y}Fe_y)_{1+z}O_2$ ($0.000 \leq y \leq 0.300$) samples. The samples of $Li_{1-z}(Ni_{1-y}Fe_y)_{1+z}O_2$ with $y = 0.025$ and 0.050 have higher first discharge capacities than $Li_{1-z}(Ni_{1-y}Fe_y)_{1+z}O_2$ with $y = 0.000$ and better or similar cycling performance at the 0.1 C rate in the voltage range of 2.7–4.2 V. Similar results have not previously been reported except for Co-substituted $LiNiO_2$. The sample $Li_{1-z}(Ni_{0.975}Fe_{0.025})_{1+z}O_2$ has the highest first discharge capacity (176.5 mAh g^{-1}). Rietveld refinement of the XRD patterns of $LiNi_{1-y}Fe_yO_2$ ($0.000 < y \leq 0.100$) from a starting structure model $[Li,Ni]_{3b}[Li,Ni,Fe]_{3a}[O_2]_{6c}$ showed that cation disordering occurred in the samples.

Keywords Lithium ion battery · $Li_{1-z}(Ni_{1-y}Fe_y)_{1+z}O_2$ · Combustion method in air · Cation disordering

M. Y. Song (✉) · I. H. Kwon
Division of Advanced Materials Engineering, Nanomaterials Processing Research Center, Engineering Research Institute, Chonbuk National University, 664-14 1ga Deogjindong Deogjingu Jeonju, 561-756, South Korea
e-mail: songmy@chonbuk.ac.kr

J. Song
Fairmont Preparatory Academy, 2200 West Sequoia Avenue, Anaheim, CA 92801, USA

J. Song
Fairmont Private Schools, Mable Campus, 1557 W. Mable Street, Anaheim, CA 92802, USA

S. Shim
Rolls-Royce Corporation, 2001 South Tibbs Ave., Speed Code W-08, Indianapolis, IN 46241, USA

1 Introduction

Transition metal oxides such as $LiMn_2O_4$ [1–3], $LiCoO_2$ [4–6] and $LiNiO_2$ [7–16] have been investigated as potential cathode materials for lithium secondary batteries. $LiMn_2O_4$ is quite inexpensive and does not bring about environmental pollution, but its cycling performance is not good. $LiCoO_2$ has a large diffusivity and a high operating voltage, and it can be easily prepared. However, it has the disadvantage that it contains an expensive element Co. $LiNiO_2$ is a very promising cathode material since it has a large discharge capacity and is excellent from the viewpoints of economics and the environment. However, its preparation is very difficult as compared with $LiCoO_2$ and $LiMn_2O_4$.

It is known that $Li_{1-z}Ni_{1+z}O_2$ forms rather than the stoichiometric $LiNiO_2$ during preparation [14, 17–19]. This phenomenon is called cation disordering. Excess nickel occupies the Li sites, destroying the ideally layered structure and preventing the easy movement of the lithium ions required for their intercalation and deintercalation during cycling. This results in a small discharge capacity and a poor cycling performance.

To improve the electrochemical properties of $LiNiO_2$, Co [20–24], Al [25–28], Ti [29–32], Ga [33], Mn [34] and Fe [35–39] ions were substituted for nickel ions by synthesis in oxygen. Reimers et al. [35] studied solid solution series of $LiFe_yNi_{1-y}O_2$ ($0.1 \leq y \leq 0.5$). They reported that the cation disordering was primarily between Fe and Li, and the

amount of Li which can be reversibly cycled decreases as y increases. Kanno et al. [36] synthesized $LiFe_{1-y}Ni_yO_2$ by the ion-exchange reaction and reported that the cycling capacities of the 4 V region decreased with increasing iron content. Prado et al. [38] studied the cation distribution in $Li_{1-z}(Ni_{1-y}Fe_y)_{1+z}O_2$ electrode materials, and reported that for the largest y and z values, iron ions are simultaneously present in the slab and in the inter-slab space. Chappel et al. [39] investigated the magnetic and structural properties of the hexagonal solid solution $LiNi_{1-y}Fe_yO_2$ ($y \leq 0.3$), and showed that 3d cations are always present in the Li layers. They also reported that Fe ions preferentially exist at the Ni site when $y \leq 0.1$.

$LiNiO_2$ synthesized by the solid-state reaction method does not have a large discharge capacity and does not exhibit good cycling performance, probably because it has poor crystallinity, and a smaller fraction of the $LiNiO_2$ phase due to the presence of impurities. On the other hand, the homogeneous mixing of the starting materials can be accomplished by the combustion method, because in this method nitrates as starting materials and urea as a fuel are mixed in distilled water by a magnetic stirrer. This may lead to good crystallinity and a homogeneous particle size when the sample is synthesized.

Combustion synthesis is based on the field of propellants and explosives. Combustion synthesis is a chemical reaction between metal salts and a suitable organic fuel. The reaction accompanies an exothermic and self-sustaining chemical reaction [40]. Its processing feature is that an amount of initial heat is required to start the chemical reaction. Subsequently, the chemical reaction supplies the energy required for the materials to react with each other without the input of external energy [41].

The range of the substituted fraction, y, in $LiNi_{1-y}M_yO_2$ of many studies was $0.0 \leq y \leq 0.9$. A review of the results of these studies showed that the charge and discharge capacities decreased rapidly when $y > 0.025$ except in the case of Co substitution. When Fe is substituted for Ni, the capacity reduction was severe when $y \geq 0.100$. For this work, we chose $0.010 \leq y \leq 0.300$ as the range of y, in which the value of y is smaller than the substituted fractions in the previously reported studies.

In this work, $Li_{1-z}(Ni_{1-y}Fe_y)_{1+z}O_2$ ($y = 0.000$, 0.010, 0.025, 0.050, 0.100 and 0.300) were synthesized by the combustion method in an air atmosphere. The electrochemical properties of the resulting compounds were then measured.

2 Experimental

In order to synthesize $Li_{1-z}(Ni_{1-y}Fe_y)_{1+z}O_2$ ($y = 0.000$, 0.010, 0.025, 0.050, 0.100 and 0.300) by the combustion method in air, lithium nitrate ($LiNO_3$, Aldrich chemical, purity 98%), nickel hexahydrate ($Ni(NO_3)_2 \cdot 6H_2O$, Aldrich chemical, purity 98%) and iron nonahydrate ($Fe(NO_3)_3 \cdot 9H_2O$, Aldrich chemical, purity 98%) were used as the starting materials. The starting materials, in the desired proportions, were mixed with urea (NH_2CONH_2, Aldrich chemical, purity 98%) as a fuel in a mole ratio of urea to nitrate 3.6 by means of a magnetic stirrer. These mixed samples were preheated in air at 400 °C for 30 min. For the synthesis of $Li_{1-z}(Ni_{1-y}Fe_y)_{1+z}O_2$ the preheated mixtures were then calcined in air at 600–800 °C for 3–48 h. The heating and cooling rates were about 100 °C h^{-1}.

The phase identification of the synthesized samples was carried out by X-ray diffraction (XRD) analysis using Cu K_α radiation. A Rigaku III/A X-ray diffractometer was used. The scanning rate was 8° min^{-1} and the scanning range of the diffraction angle (2θ) was $10° \leq 2\theta \leq 80°$. The resulting peaks were refined by the Rietveld method using GSAS program [42]. The peak shape was described by a pseudo-Voigt function. For each diffraction pattern, the scale factor, zero point, unit-cell dimensions, and atomic parameters were refined. The morphologies of the samples were observed by a field emission-scanning electron microscope (FE-SEM). The materials before combustion have limitations on analysis because of their strong exothermic reactions. In order to investigate the phase transitions of the materials, thus DTA (differential thermal analysis, TA Instruments Inc. 1600 DTA) was performed for $Li_{1-z}Ni_{1+z}O_2$ precursor (an intermediate) combusted at 400 °C for 30 min and FTIR analysis (MB100, ABB BOMEN) for the samples (products) calcined after combustion at 400 °C for 30 min.

To measure the electrochemical properties, electrochemical cells were constructed consisting of the prepared sample as the positive electrode, Li metal as the negative electrode, and 1 M $LiPF_6$ in a 1:1 (volume ratio) mixture of ethylene carbonate (EC) and diethyl carbonate (DEC) as the electrolyte. A Whatman glass fiber was used as a separator. The cells were assembled in an argon-filled dry box. To fabricate the positive electrode, the active material, acetylene black and polyvinylidene fluoride (PVDF) binder dissolved in *N*-methyl-2-pyrrolidone (NMP) were mixed at a weight ratio of 85:10:5 and applied on Al foil. All the electrochemical tests were performed at room temperature with a battery charge–discharge cycle tester at the 0.1 C rate in the voltage ranges between 2.7 and 4.9 V.

3 Results and discussion

Figure 1 shows the X-ray powder diffraction patterns of $Li_{1-z}Ni_{1+z}O_2$ calcined in air at 600–800 °C for 3–48 h after preheating in air at 400 °C for 30 min. The samples

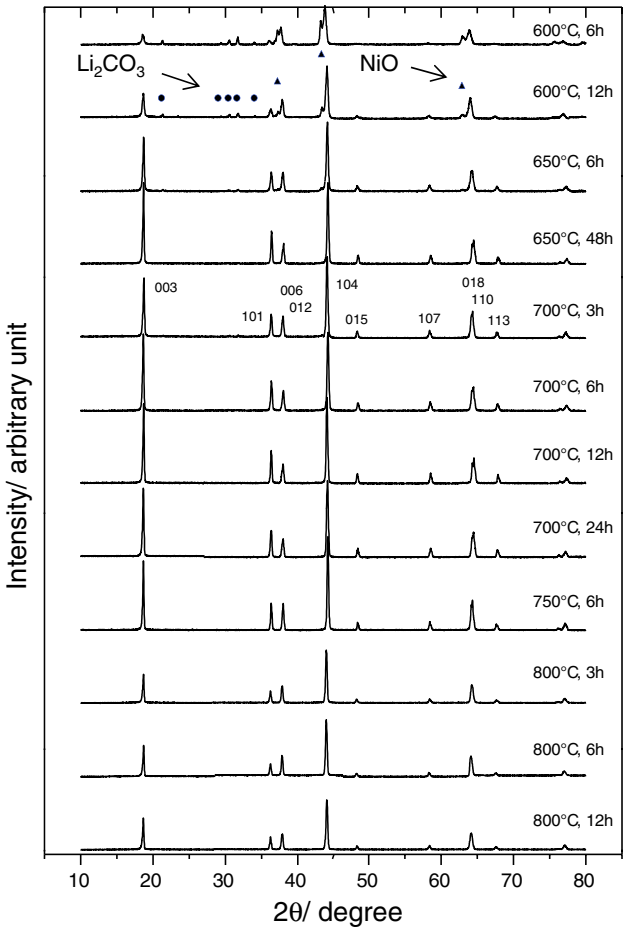

Fig. 1 XRD patterns of $Li_{1-z}Ni_{1+z}O_2$ synthesized by the combustion method in air at various temperatures for various times

calcined at 600 and 650 °C have a phase with an α-$NaFeO_2$ structure (space group; $R\bar{3}m$), but they also contain NiO and Li_2CO_3 except the sample calcined for 48 h. As the calcination time increases, the intensities of the peaks for the α-$NaFeO_2$ structure increase, while those for NiO and Li_2CO_3 decrease. The α-$NaFeO_2$ structure with good crystallinity has more intense 101 peak than the 012 peak. However, in the samples calcined at 750 and 800 °C the intensity of the 101 peak was similar to or weaker than that of the 012 peak. Moreover, the samples calcined at 800 °C showed less intense peaks than those calcined at 700 °C. The sample calcined at 700 °C for 3 h contains Li_2CO_3, but the samples calcined at 700 °C for 6 h or more do not contain any un-reacted materials and have similar X-ray diffraction patterns, with the 101 peak being more intense than the 012 peak. Morales et al. [17] correlated semi-quantitatively the integrated intensity ratio of the 003 and 104 peaks with the lithium content in samples with $x < 0.9$. The ratio was later used by Ohzuku et al. [43] as a qualitative criterion for the stoichiometry of samples with $x > 0.96$. It is known that the cation disordering decreases as the value of I_{003}/I_{104} increases. The values of I_{003}/I_{104} were 0.74, 0.98, 0.92 and 0.91 for the samples calcined for 3, 6, 12 and 24 h, respectively, showing that I_{003}/I_{104} value initially increases with increasing calcination time before tailing off. This shows that the cation disordering decreases as the calcination time increases from 3 h to 6, 12 and 24 h.

Rietveld refinement was performed in order to evaluate the influence of calcining condition on the cation disordering. Since the radius of Li^+ (0.76 Å) and Ni^{2+} cation (0.69 Å) is similar, Ni and Li atoms are allowed to exchange 3a and 3b site. Hence, $[Li,Ni]_{3b}[Li,Ni]_{3a}[O_2]_{6c}$ model was used for the refinement. The Rietveld analysis results of $Li_{1-z}Ni_{1+z}O_2$ calcined at 700 °C for various times are summarized in Table 1. Overall, the refinement gave good agreement factors represented by R_p, R_{pw}, and R_b. Especially, low R_b values, 2–3%, indicates that the structure model is robust. As calcining temperature increases above 700 °C, cation disordering, Ni migration from 3a site to 3b site, became more prominent. When powder was calcined at 700 °C, cation disordering was reduced as the heat treatment time increases, from 3 to 12 and 24 h. This agrees well with the behavior of the I_{003}/I_{104} value with the hold time mentioned above. According to this result, it can be deduced that controlling calcining temperature and hold time is crucial to synthesize good α-$NaFeO_2$ structured $Li_{1-z}Ni_{1+z}O_2$.

Figure 2 shows the DTA curve of the mixture for the synthesis of lithium nickel oxide combusted at 400 °C for 30 min. The peaks for the exothermic reaction are observed at about 500 and 675 °C, and the peak for the endothermic reaction at around 735 °C. Figure 1 showed that the sample calcined at 750 °C for 6 h contained a phase with the α-$NaFeO_2$ structure, NiO and Li_2CO_3. The sample calcined at 650 °C for 6 h still contained a small amount of NiO and Li_2CO_3, but they both disappeared after calcination for 48 h. The sample calcined at 700 °C for 6 h contained only the phase with the α-$NaFeO_2$ structure. In the samples calcined at and above 750 °C, the values of I_{003}/I_{104} decreased, indicating the increase in the cation disordering. From these results, the peak at about 500 °C is considered to correspond to the formation of NiO, and the peak at about 675 °C to the temperature of the practical completion of the formation of lithium nickel oxide. The strong endothermic peak at about 735 °C is considered to be from the melting of Li_2CO_3 present in the sample.

For the syntheses of $LiNi_{1-y}Fe_yO_2$ ($0.000 \leq y \leq 0.300$), mixtures of the starting materials with the desired compositions were calcined in an air atmosphere at 700 °C for 48 h after preheating them in air at 400 °C for 30 min.

Figure 3 shows the X-ray powder diffraction patterns of $Li_{1-z}(Ni_{1-y}Fe_y)_{1+z}O_2$ ($0.000 \leq y \leq 0.300$) calcined in air at 700 °C for 48 h after preheating in air at 400 °C for 30 min. All of the samples except the sample with

Table 1 Rietveld analysis results of $Li_{1-z}Ni_{1+z}O_2$ calcined at 700 °C for various times

Sample		R_p R_{pw} (%) R_b	a/Å	c/Å	c/a	Li_{3b}	Ni_{3b}	Li_{3a}	Ni_{3a}
700 °C	3 h	7.7							
		9.0	2.890	14.221	4.920	0.8041	0.1959	0.0794	0.9206
		3.0							
700 °C	12 h	7.2							
		9.1	2.885	14.214	4.927	0.8523	0.1477	0.0587	0.9413
		2.1							
700 °C	24 h	7.7							
		10.2	2.889	14.226	4.924	0.8539	0.1403	0.0664	0.9336
		2.2							
750 °C	6 h	9.1							
		7.5	2.893	14.229	4.919	0.7916	0.2084	0.0637	0.9363
		2.2							
800 °C	12 h	7.5							
		9.6	2.895	14.235	4.917	0.7248	0.2752	0.0549	0.9451
		3.3							

$y = 0.300$ have the phase with the α-$NaFeO_2$ structure of the rhombohedral system (space group; $R\bar{3}m$). These samples exhibit distinct splitting between the 006 and 012 peaks and between the 018 and 110 peaks, suggesting that they have a well-developed 2D layer structure and are electrochemically active [43]. It has been reported that Fe^{3+} occupies the Ni sites preferentially, compared to Ni^{2+} when Fe composition in Ni site is less than 0.1 [39]. Therefore, Rietveld refinement was carried out from a starting structure model $[Li,Ni]_{3b}[Li,Ni,Fe]_{3a}[O_2]_{6c}$, assuming Fe does not migrate to Li site. In Table 2, Rietveld analysis results for $Li_{1-z}(Ni_{1-y}Fe_y)_{1+z}O_2$ $(0 \leq y \leq 0.100)$ calcined in air at 700 °C for 48 h is summarized. The entire XRD patterns were well fitted by the proposed structure model. Both *a* and *c* calculated from refinement increased linearly with the increase of Fe content. *c/a* ratio also increased with more Fe content except when $y = 0.025$. The degree of cation disordering was represented by Ni occupancy at 3b site. Cation disordering was minimum at $y = 0.010$ and maximum at $y = 0.100$. More cation disordering was observed from $y = 0.025$ and 0.050 samples when they are compared to $Li_{1-z}Ni_{1+z}O_2$, indicating that Fe addition more than 0.010 does not improve cation disordering.

Figure 4 shows the FE-SEM photographs of $Li_{1-z}(Ni_{1-y}Fe_y)_{1+z}O_2$ $(0.000 \leq y \leq 0.300)$ calcined in air at 700 °C for 48 h. All of the samples have particles with edges. The sample with $y = 0.000$ has the smallest particles. The particles of the samples with $y = 0.010$, 0.025 and 0.050 have similar and relatively uniform sizes of about 1 μm. The samples with $y = 0.100$ and $y = 0.300$

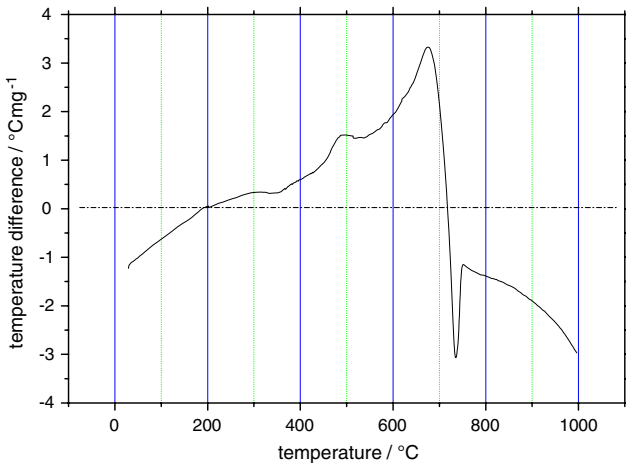

Fig. 2 DTA curve of $Li_{1-z}Ni_{1+z}O_2$ precursor combusted at 400 °C for 30 min

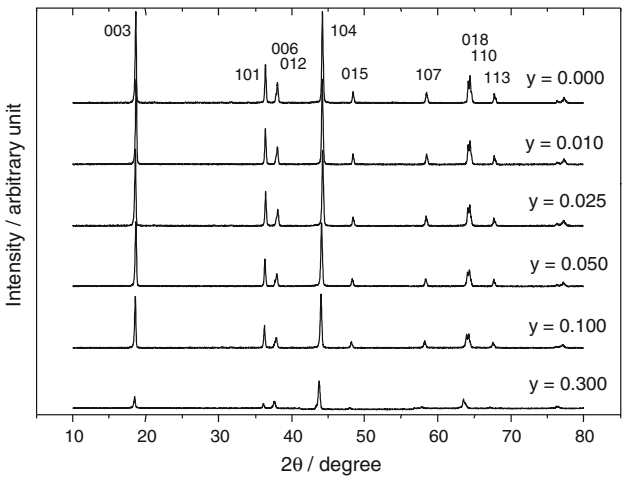

Fig. 3 XRD patterns of $Li_{1-z}(Ni_{1-y}Fe_y)_{1+z}O_2$ $(0.000 \leq y \leq 0.300)$ calcined in air at 700 °C for 48 h

Table 2 Rietveld analysis results for $Li_{1-z}(Ni_{1-y}Fe_y)_{1+z}O_2$ ($0 \leq y \leq 0.100$) calcined in air at 700 °C for 48 h

Sample	R_p R_{pw} (%) R_b	a/Å	c/Å	c/a	Li_{3b}	Ni_{3b}	Li_{3a}	Ni_{3a}	Fe_{3a}
$y = 0.000$	9.4								
	11.3	2.883	14.208	4.928	0.8860	0.1140	0.0515	0.9485	0.0000
	2.5								
$y = 0.010$	8.8								
	11.2	2.884	14.214	4.929	0.8915	0.1085	0.0713	0.9187	0.0100
	3.1								
$y = 0.025$	10.2								
	12.5	2.885	14.215	4.928	0.8768	0.1232	0.0660	0.9090	0.0250
	3.5								
$y = 0.050$	9.9								
	12.1	2.887	14.232	4.930	0.8782	0.1218	0.0541	0.8959	0.0500
	3.4								
$y = 0.100$	12.7								
	15.6	2.891	14.262	4.934	0.8539	0.1461	0.0808	0.8182	0.1000
	3.8								

have larger particles than all the other samples, and the sample with $y = 0.300$ has the largest particles with a diameter of 3–5 μm. The morphologies of the sample with $y = 0.100$ and 0.300 are quite different from those of the samples with $0.000 \leq y \leq 0.100$. The particle size and morphology differences in addition to the difference in the intrinsic composition might be related to the different electrochemical performances.

Figure 5 shows the voltage versus capacity curves for the first charge and discharge of $Li_{1-z}(Ni_{1-y}Fe_y)_{1+z}O_2$ ($0.000 \leq y \leq 0.300$) calcined in air at 700 °C for 48 h. The sample with $y = 0.025$ has the highest first charge capacity (251.8 mAh g^{-1}), and the first discharge capacities decrease in the order of $y = 0.025$, 0.050, 0.000, 0.010 and 0.100. Figure 4 showed that the samples with $y = 0.000$, 0.010, 0.025 and 0.050 have similar morphologies, but the morphologies of the samples with $y = 0.100$ and 0.300 are quite different from the other samples. The different electrochemical performances observed might be related to particle size/morphology differences in addition to the difference in the intrinsic composition.

Figure 6 shows the charge capacity, discharge capacity and irreversible capacity for the first cycle of $Li_{1-z}(Ni_{1-y}Fe_y)_{1+z}O_2$ ($0.000 \leq y \leq 0.100$) calcined in air at 700 °C for 48 h in the voltage range of 2.7–4.2 V. The sample with $y = 0.025$ has the highest charge capacity (251.8 mAh g^{-1}), followed by the sample with $y = 0.050$. The sample with $y = 0.025$ has the highest discharge capacity (176.5 mAh g^{-1}), along with the smallest irreversible capacity. The sample with $y = 0.100$ has the smallest charge and discharge capacities, along with the highest irreversible capacity. When the synthesis is conducted in air, the samples $Li_{1-z}(Ni_{1-y}Fe_y)_{1+z}O_2$ ($y = 0.025$ and 0.050) have higher discharge capacities than $Li_{1-z}Ni_{1+z}O_2$. Similar results have not previously been reported except in the case of Co-substituted $LiNiO_2$. In the $LiNiO_2$ phase, Li occupies the 3b sites, Ni the 3a sites and O the 6c sites, where 3b, 3a, and 6c refer to the sites defined in the hexagonal setting of the space group $R\bar{3}m$. The irreversible capacities are quite high for all of the samples, indicating that the quantity of intercalated Li^+ in the first discharge is much smaller than that of deintercalated Li^+ in the first charge. It is considered that this is because, during the first charge, Li ions not only deintercalate from the 3b sites but also come out from the Li atoms which may be contained in the unstable $Li_{1-z}Ni_{1+z}O_2$ phase or which are present in excess outside the 3b sites within the sample. During the first charge, the deintercalation of Li ions from the unstable 3b sites may destroy the $Li_{1-z}Ni_{1+z}O_2$ structure (α-$NaFeO_2$ structure) and the quantity of intercalating Li ions in the first discharge will be smaller.

Figure 7 shows the $-dx/|dV|$ vs. voltage curve for the 1st cycle of $Li_{1-z}(Ni_{1-y}Fe_y)_{1+z}O_2$ ($y = 0.000$ and 0.025) calcined in air at 700 °C for 48 h. The sharp peak corresponds to a phase transition at which two phases co-exist and the broad peak corresponds to a phase transition at which one-phase changes continuously [44]. The curves in Fig. 8 show that the peaks ascribable to the formation intermediate phases are not clearly resolved, thus meaning that their products are highly non-stoichiometric [45]. During charging, $Li_{1-z}Ni_{1+z}O_2$ exhibits behavior similar to that of the sample with $y = 0.025$ except that the former has peaks at higher voltages than the latter. But during discharging, $Li_{1-z}Ni_{1+z}O_2$ shows a phase transition at a lower voltage, whereas the sample with $y = 0.025$ exhibits two phase

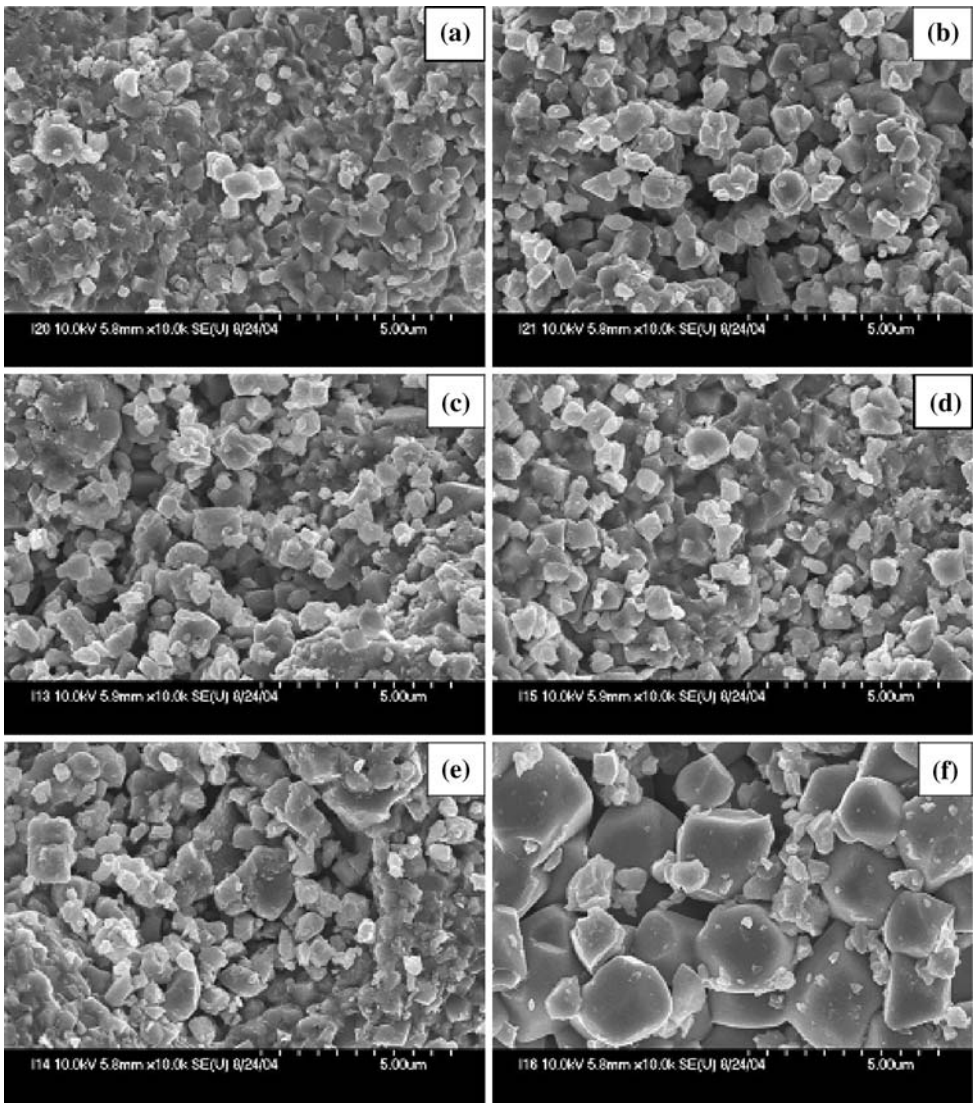

Fig. 4 FE-SEM photographs of $Li_{1-z}(Ni_{1-y}Fe_y)_{1+z}O_2$ ($0.000 \leq y \leq 0.300$) calcined in air at 700 °C for 48 h; **a** $y = 0.000$, **b** $y = 0.010$, **c** $y = 0.025$, **d** $y = 0.050$, **e** $y = 0.100$ and **f** $y = 0.300$

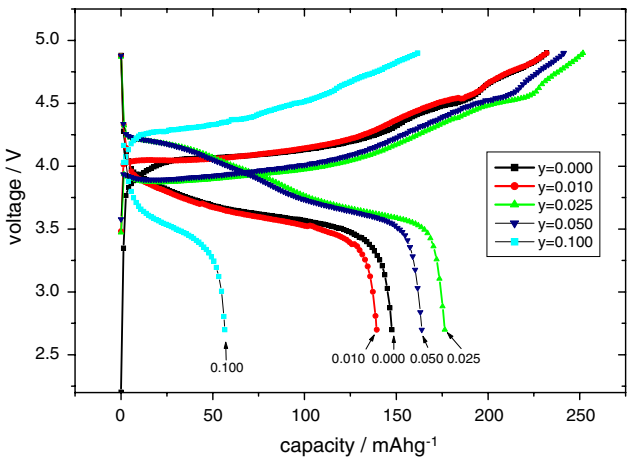

Fig. 5 First charge–discharge capacity curves for $Li_{1-z}(Ni_{1-y}Fe_y)_{1+z}O_2$ ($0.000 \leq y \leq 0.100$) calcined in air at 700 °C for 48 h

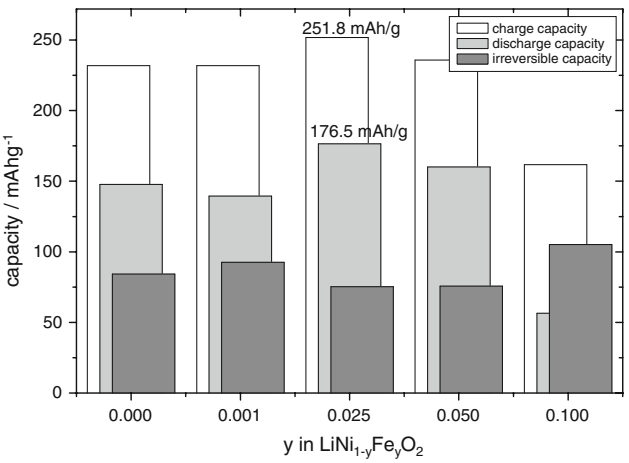

Fig. 6 First charge–discharge and irreversible capacity for $Li_{1-z}(Ni_{1-y}Fe_y)_{1+z}O_2$ ($0.000 \leq y \leq 0.100$) calcined in air at 700 °C for 48 h

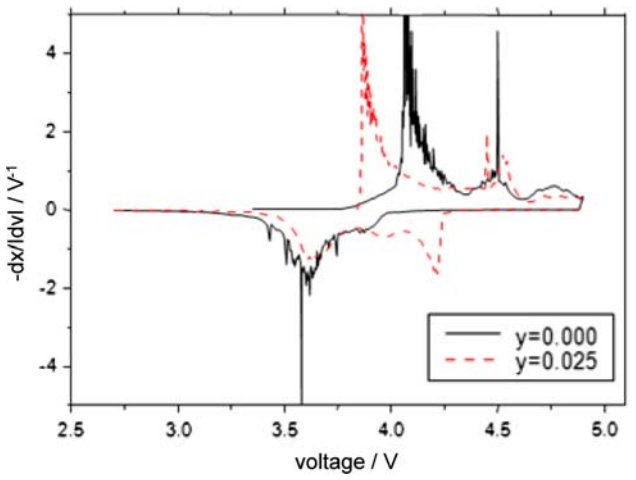

Fig. 7 Variation, with y ($y = 0.000$ and 0.025), of the derivative $-dx/|dV|$ vs. V curve for the first cycle, where x denotes the value of x in $Li_xNi_{1-y}Fe_yO_2$ calcined in air at 700 °C for 48 h

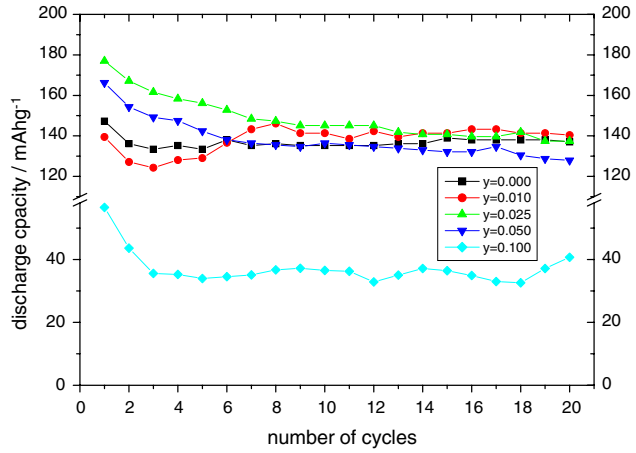

Fig. 8 Variations of discharge capacity with the number of cycles for $Li_{1-z}(Ni_{1-y}Fe_y)_{1+z}O_2$ ($0.000 \leq y \leq 0.100$) calcined in air at 700 °C for 48 h

transitions. This shows that $Li_{1-z}Ni_{1+z}O_2$ has more sites that are inactive electrochemically, due to the existence of more Ni^{+2} ions in the Li sites, than the sample with $y = 0.025$, even though both samples are highly non-stoichiometric. The Ni^{+2} ions in the Li sites are inactive electrochemically and disturb the diffusion of Li^+, resulting in the prevention of the phase transformation related to the intercalation and deintercalation.

Figure 8 shows the variations of the discharge capacity at the 0.1 C rate with the number of cycles, n, for the $Li_{1-z}(Ni_{1-y}Fe_y)_{1+z}O_2$ ($0.000 \leq y \leq 0.100$) calcined in air at 700 °C for 48 h in the voltage range of 2.7–4.2 V. The first discharge capacity decreases in the order of the samples with $y = 0.025$, 0.050, 0.000, 0.010 and 0.100. The discharge capacity of $Li_{1-z}Ni_{1+z}O_2$ decreases at the second cycle, but remains almost constant thereafter. The discharge capacity of the sample with $y = 0.010$ decreases up to $n = 3$, then increases up to $n = 7$, and does not vary thereafter. The increase in the discharge capacity from to $n = 3$ up to $n = 7$ is considered because some sites are aged or activated for intercalation and deintercalation with charge–discharge cycling. The discharge capacities of the samples with $y = 0.025$ and 0.050 decrease gradually as the number of cycles increases. The sample with $y = 0.100$ has the smallest first discharge capacity of 56.6 mA h/g and its discharge capacity decreases with increasing n. Choi et al. [46] investigated the effects of cation disordering on electrochemical lithium intercalation involving the absorption reaction and diffusion of lithium ion in porous $Li_{1-\delta}Ni_{1-y}Co_yO_2$ electrodes ($0 \leq \delta$; $y \leq 1$) by using electrochemical impedance spectroscopy (EIS), and reported that the substituted Co ($0.2 \leq y \leq 0.3$) decreases the lattice size and makes the Ni^{2+} ions, which are larger than Ni^{3+} ions, unstable. This prevents the Ni^{2+} ions from entering the Li sites and leads to the formation of $Li_{1-z}(Ni_{1-y}Co_y)_{1+z}O_2$ with z = nearly zero, resulting in better electrochemical properties. Prado et al. [47] reported that the substitution of Fe for Ni in $LiNiO_2$ degrades the electrochemical properties, by making the lattice size larger and thus making the Ni^{2+} ions more stable than Ni^{3+}. However, the samples with $y = 0.025$ and 0.050 in this work have higher first discharge capacities than $Li_{1-z}Ni_{1+z}O_2$ and better or similar cycling performance. In addition, the samples with $y = 0.025$ and 0.050 in this work have higher discharge capacities than $Li_{1-z}Ni_{1+z}O_2$ and cycling performances similar to that of $Li_{1-z}Ni_{1+z}O_2$ from $n = 7$ through $n = 20$. The samples with $y = 0.000$, 0.010, 0.025 and 0.050 have much higher discharge capacities than the sample with $y = 0.100$ from $n = 1$ through $n = 20$. They show similar discharge capacities and good cycling performances from $n = 7$ through $n = 20$. The samples with $y = 0.000$, 0.010, 0.025 and 0.050 showed similar and larger Li occupancy at 3b site (similar and smaller cation disordering) than the sample with $y = 0.100$ (Table 2).

Figure 9 shows the FTIR desorbance curves in the ranges of wave number of (a) 400–1,800 cm^{-1} and (b) 400–800 cm^{-1} (in a magnified scale) for $Li_{1-z}(Ni_{1-y}Fe_y)_{1+z}O_2$ ($y = 0.000$, 0.025 and 0.100) calcined in air at 700 °C for 48 h. All of the samples exhibit one peak and two peaks in the ranges of wave number of 800–900 cm^{-1} and 1,400–1,600 cm^{-1}, respectively. These peaks correspond to CO_3^{2-}, indicating that some Li_2CO_3 remains in the samples. The two peaks in the range of wave number lower than 600 cm^{-1}, observed for all of the samples, correspond to the M–O–M bond. The sample with $y = 0.100$ shows wider peaks than the other samples. This is related to the increase of disordering in the lattice (entrance of Ni^{2+} ions to the Li sites) with the increase of z in $Li_{1-z}(Ni_{1-y}Fe_y)_{1+z}O_2$ [48]. The differences in the intensities of the two peaks in the range of wave number lower than 600 cm^{-1} are 0.041,

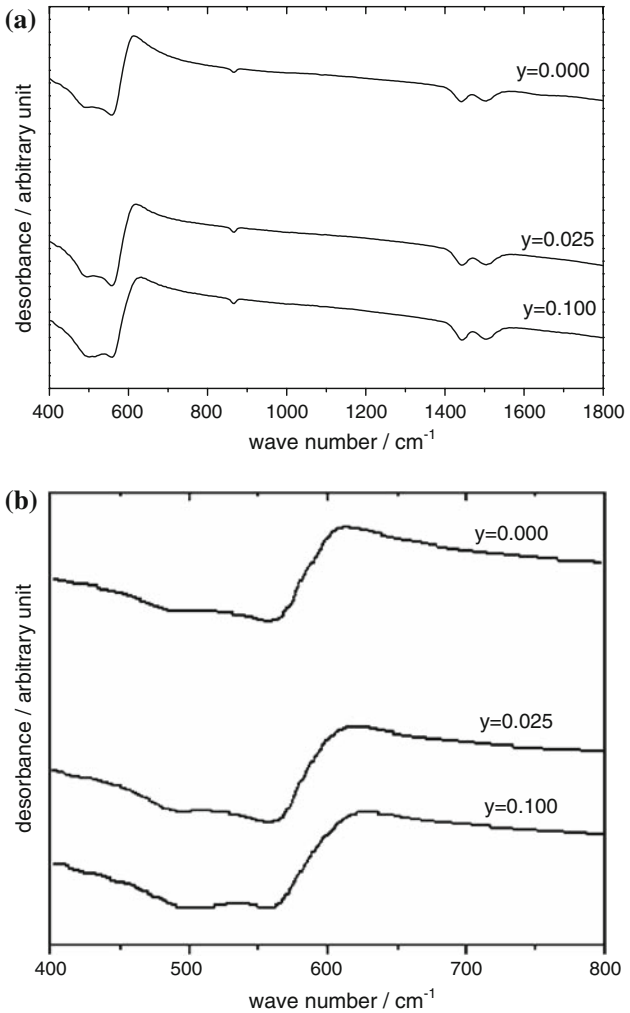

Fig. 9 FTIR desorbance curves in the ranges of wave number of **a** 400–1,800 cm^{-1} and **b** 400–800 cm^{-1} for $Li_{1-z}(Ni_{1-y}Fe_y)_{1+z}O_2$ (y =0.000, 0.025 and 0.100) calcined in air at 700 °C for 48 h

3.521 and 2.944 for the samples with $y = 0.000$, 0.025 and 0.100, respectively, with the sample with $y = 0.025$ having the highest value. In the case where $LiNi_{1-y}Co_yO_2$ was synthesized under optimum conditions for obtaining a nearly stoichiometric composition, the peaks became narrower and the difference in the intensities of these two peaks became larger [49, 50]. Thus, when $Li_{1-z}(Ni_{1-y}Fe_y)_{1+z}O_2$ is synthesized in air, the sample with $y = 0.025$ has less defects than $Li_{1-z}Ni_{1+z}O_2$ and accordingly has better structural stability and electrochemical properties.

4 Conclusions

Rietveld refinement of the XRD patterns of $Li_{1-z}Ni_{1+z}O_2$ calcined at 700 °C for various times was carried out from a starting structure model $[Li,Ni]_{3b}[Li,Ni]_{3a}[O_2]_{6c}$ model. It showed that when powder was calcined at 700 °C, cation disordering was reduced as the heat treatment time increases, from 3 to 12 and 24 h, agreeing well with the behavior of the I_{003}/I_{104} value with the hold time. The phases appearing in the intermediate reaction steps for the formation of lithium nickel oxide are deduced from the XRD patterns and the DTA analysis. The particles of the samples with $y = 0.010$, 0.025 and 0.050 have similar and relatively uniform sizes of about 1 μm. The $-dx/|dV|$ vs. voltage curve for the 1st cycle of $Li_{1-z}(Ni_{1-y}Fe_y)_{1+z}O_2$ ($y = 0.000$ and 0.025) shows that $Li_{1-z}Ni_{1+z}O_2$ has more sites that are inactive electrochemically, due to the existence of more Ni^{+2} ions in the Li sites, than the sample with $y = 0.025$. The samples of $Li_{1-z}(Ni_{1-y}Fe_y)_{1+z}O_2$ with $y = 0.025$ and 0.050 have higher first discharge capacities than $Li_{1-z}Ni_{1+z}O_2$ and better or similar cycling performance at the 0.1 C rate in the voltage range of 2.7–4.2 V. Similar results have not previously been reported except in the case of Co-substituted $LiNiO_2$. The sample $Li_{1-z}(Ni_{0.975}Fe_{0.025})_{1+z}O_2$ has the highest first charge capacity (251.8 mAh g^{-1}) and the highest first discharge capacity (176.5 mAh g^{-1}).

References

1. Tarascon JM, Wang E, Shokoohi FK, McKinnon WR, Colson S (1991) J Electrochem Soc 138:2859
2. Armstrong AR, Bruce PG (1996) Nature 381:499
3. Ahn DS, Song MY (2000) J Electrochem Soc 147(3):874
4. Ozawa K (1994) Solid State Ionics 69:212
5. Alcátara R, Lavela P, Tirado JL, Stoyanova R, Zhecheva E (1997) J Solid State Chem 134:265
6. Peng ZS, Wan CR, Jiang CY (1998) J Power Sources 72:215
7. Dahn JR, von Sacken U, Michal CA (1990) Solid State Ionics 44:87
8. Dahn JR, von Sacken U, Juzkow MW, Al-Janaby H (1991) J Electrochem Soc 138:2207
9. Marini A, Massarotti V, Berbenni V, Capsoni D, Riccardi R, Antolini E, Passalacqua B (1991) Solid State Ionics 45:143
10. Ebner W, Fouchard D, Xie L (1994) Solid State Ionics 69:238
11. Kanno R, Kubo H, Kawamoto Y, Kamiyama T, Izumi F, Takeda Y, Takano M (1994) J Solid State Chem 110:216
12. Hirano A, Kanno R, Kawamoto Y, Takeda Y, Yamaura K, Takano M, Ohyama K, Ohashi M, Yamaguchi Y (1995) Solid State Ionics 78:123
13. Rougier A, Gravereau P, Delmas C (1996) J Electrochem Soc 143:1168
14. Arai H, Okada S, Sakurai Y, Yamaki J (1997) Solid State Ionics 95:275
15. Song MY, Lee R (2002) J Power Sources 111(1):97
16. Song MY, Kwon IK, Kim HU, Shim S, Mumm DR (2006) J Appl Electrochem 36:801
17. Morales J, Perez-Vicente C, Tirado JL (1990) Mater Res Bull 25:623
18. Arai H, Okada S, Ohtsuka H, Ichimura M, Yamaki J (1995) Solid State Ionics 80:261
19. Ksenofontov V, Reiman S, Walcher D, Garcia Y, Doroshenko N, Gutlich P (2002) Hyperfine Interact 139/140:107

20. Caurant D, Baffier N, Garcia B, Pereira-Ramos JP (1996) Solid State Ionics 91:45
21. Rougier A, Saadoune I, Gravereau P, Willmann P, Delmas C (1996) Solid State Ionics 90:83
22. Lee KK, Kim KB (2000) J Electrochem Soc 147(5):1709
23. Fey GT-K, Yo WH, Chang YC (2002) J Power Sources 105:82
24. Song MY, Kwon IH, Kim HU (2005) J Appl Electrochem 35:1073
25. Guilmard M, Rougier A, Grune M, Croguennec L, Delmas C (2003) J Power Sources 115:305
26. Song MY, Lee R, Kwon IH (2003) Solid State Ionics 156:319
27. Amriou T, Sayede A, Khelifa B, Mathieu C, Aourag H (2004) J Power Sources 130:213
28. Shinova E, Zhecheva E, Stoyanova R, Bromiley GD, Alcántara R, Tirado JL (2005) J Solid State Chem 178:2692
29. Chang SH, Kang SG, Song SW, Yoon JB, Choy JH (1996) Solid State Ionics 86–88:171
30. Gao Y, Yakovleva MV, Ebner WB (1998) Electrochem Solid-State Lett 1:117
31. Kim J, Amine K (2001) Electrochem Commun 3:52
32. Kim J, Amine K (2002) J Power Sources 104:33
33. Nishida Y, Nakane K, Stoh T (1997) J Power Sources 68:561
34. Guilmard M, Croguennec L, Delmas C (2003) J Electrochem Soc 150(10):A1287
35. Reimers JN, Rossen E, Jones CD, Dahn JR (1993) Solid State Ionics 61:335
36. Kanno R, Shirane T, Inaba Y, Kawamoto Y (1997) J Power Sources 68:145
37. Song MY, Ahn DS (1998) Solid State Ionics 112:245
38. Prado G, Suard E, Fournes L, Delmas C (2000) J Mater Chem 10:2553
39. Chappel E, Chouteau G, Prado G, Delmas C (2003) Solid State Ionics 159:273
40. Jain SR, Adiga KC, Pai Verneker V (1981) Combust Flame 40:71
41. Zhang Y, Stangle GC (1994) J Mater Res 9:1997
42. Larson A, von Dreele RB (1994) Los Alamos Laboratory Report
43. Ohzuku T, Ueda A, Nagayama M (1993) J Electrochem Soc 140:1862
44. Li W, Reimers JN, Dahn JR (1993) Solid State Ionics 67:123
45. Alcántara R, Lavela P, Tirado JL (1997) Chem Mater 9:2145
46. Choi YM, Pyun SI, Moon SI (1996) Solid State Ionics 89:43
47. Prado G, Rougier A, Fournes L, Delmas C (2000) J Electrochem Soc 147(8):2880
48. Lin SP, Fung KZ, Hon YM, Hon MH (2001) J Cryst Growth 226:148
49. Julien C, Michael SS, Ziolkiewicz S (1999) Int J Inorg Mater 1:29
50. Kalyani P, Kalaiselvi N, Renganathan NG, Raghavan M (2004) Mater Res Bull 39:41